Interactions between the Space Environment and Ganymede's Surface

A. Galli, A. Vorburger, P. Wurz, Marina Galand, Apurva Oza, Shahab Fatemi, Christina Plainaki, Alessandro Mura

1. Introduction

Because Ganymede lacks a substantial atmosphere, its surface is exposed to the harsh space environment in the Jovian magnetosphere. Generally speaking, the space environment interacts with and alters the surface of any air-less icy moon via four processes:

1. Sputtering and radiolysis by particle irradiation
2. Thermal sublimation
3. Micrometeoroid impacts
4. Photo-stimulated desorption

These interaction processes are important both for the surface itself and as sources for the neutral atmosphere and the ionosphere of Ganymede. *The latter two will be covered in detail in subsequent chapters 3.3. (atmosphere) and 3.4 (ionosphere).* The focus of this chapter lies on the surface interaction processes themselves.

Most studies on Ganymede's surface alteration and atmosphere release processes concentrate on the first two processes. Photo-stimulated desorption and micrometeoroids are usually neglected as a source for neutral atmosphere models (Marconi, 2007; Khurana et al., 2007; Turc et al., 2014; Plainaki et al., 2015; Fatemi et al., 2016; Leblanc et al., 2017; Shematovich et al., 2016; Plainaki et al., 2020a,b). This approach was motivated by Marconi (2007); Shematovich et al. (2016), e.g., who **considered the widespread coverage of water-ice on the surface an indication that sublimation of water ice and sputtering of water-ice by magnetospheric ions are the main sources for Ganymede's atmosphere. Shematovich et al. (2016) also predicted sputtering to dominate in the polar**

regions, wherease sublimation should dominate in the equatorial regions near the subsolar point. We will come back to this question about relative importance of processes in the next section.

Section 2 of this chapter defines and describes the four interaction processes in more detail. Section 3 is dedicated to the most complex of the four processes, irradiation caused by charged particles. Section 4 discusses the role of the different interactions for some Ganymede surface features. Section 5 gives a compact summary of the chapter.

2. Overview of Surface Interaction Processes on Ganymede

Before explaining the details of the four surface interactions, we attempt to compare the relative importance of irradiation (i.e., sputtering and radiolysis), sublimation, micrometeoroid impacts, and desorption on Ganymede's surface. This can be done in many different ways, depending on the specific science question at hand. Given the lack of accurate numbers and the sheer complexity of the interactions we restrict ourselves to the case most investigated in recent surface and atmosphere: the erosion or turnover rate of water ice on the surface of Ganymede, expressed as removed ice in μm yr^{-1} (in analogy to Cooper et al. (2001); Johnson et al. (2004)).

The results are summarized in Fig. 1 and in Table 1. Photo-stimulated desorption is negligible for water ice removal compared to the three other processes everywhere on Ganymede's surface, whereas irradiation, sublimation, and micrometeoroid impacts may all turn out relevant at different specific surface areas. This can be recognized in Fig. 1 as follows: Where T always remains below 120 K, micrometeoroid impacts and irradiation dominate. For 120 to 130 K (typically around 45° latitude during illumination) sublimation amounts to a comparable order of magnitude. Wherever T exceeds 130 K sometimes during the orbit, sublimation removes water ice much faster than any other process. At the warmest region (150 K) about 600 μm yr^{-1} of water ice would be removed compared to the $0.1 \ldots 1$ μm yr^{-1} removed by micrometeoroids and irradiation combined!

The total release rates related to irradiation are **dominated by ion sputtering (see Section 3.2.1) and amount to** 10^{26} to 10^{27} s^{-1} according to recent models by Carnielli et al. (2020); Poppe et al. (2018); Plainaki et al. (2020a) (with the exception of the ionospheric boost case by Carnielli et al. (2020), see Section 3.1). This order of magnitude translates into $0.01 \ldots 0.1$ μm yr^{-1} under the assumption that the ions precipitate onto the 50% of

Table 1: Water ice removal or turnover rates on Ganymede's surface in equatorial (Equ.) and polar regions in units of μm yr^{-1} (last three columns). References for ion irradiation: (Carnielli et al., 2020; Poppe et al., 2018; Plainaki et al., 2020a), **rates from electron irradiation are not quantifiable yet, but expected to be smaller**. References for micrometeoroid impacts: Cooper et al. (2001); Johnson et al. (2004); Krüger et al. (2000). References for sublimation: Bohren and Albrecht (1998); Andreas (2007).

Region	Temperature	Irradiation (ions)	Thermal sublimation	Meteoroid impacts
Equ., leading, dayside	125 ... 150 K	0.025	0.1 ... 600	0.6
Polar (lat. $> 45°$)	100 ... 125 K	0.1	< 0.001 ... 0.1	0.3
Equ., trailing, nightside	110 K	0.01	< 0.001	0.15

Ganymede's surface at high latitudes, outside the closed magnetic field lines. The transition from closed to open magnetic field lines occurs at roughly 30° latitude on the leading and roughly 45° on the trailing hemisphere as depicted in Fig. 1.

Figure 1 depicts the case that the illuminated hemisphere of Ganymede co-aligns with the leading hemisphere on the orbit around Jupiter. This is relevant because the precipitation of ions and electrons discriminates between upstream/trailing and downstream/leading hemisphere. When the trailing hemisphere is illuminated instead, the orange shape of erosion rates would flip around the vertical plot axis.

Figure 1 and Table 1 include only surface release or turnover rates. For the chemical evolution of Ganymede's surface, radiolysis and sputtering play a major role, too. Also keep in mind that the **values** in Table 1 apply to pure water ice on Ganymede. For the other, more refractory, materials present on the surface, we can assume that the erosion and turnover rate are dominated by micrometeoroids everywhere once the hydrated forms of salts and acids stable under irradiation have formed (see Section 3.2.2).

2.1. Sputtering and Radiolysis by Irradiation

Irradiation processes induced by charged particles are important both for the surface and the generation of the tenuous atmosphere of Ganymede (Marconi, 2007; Shematovich et al., 2016). For our purposes, we group irradiation processes into two broad categories: sputtering and radiolysis. Sputtering describes the ejection of surface species by an impacting energetic particle.

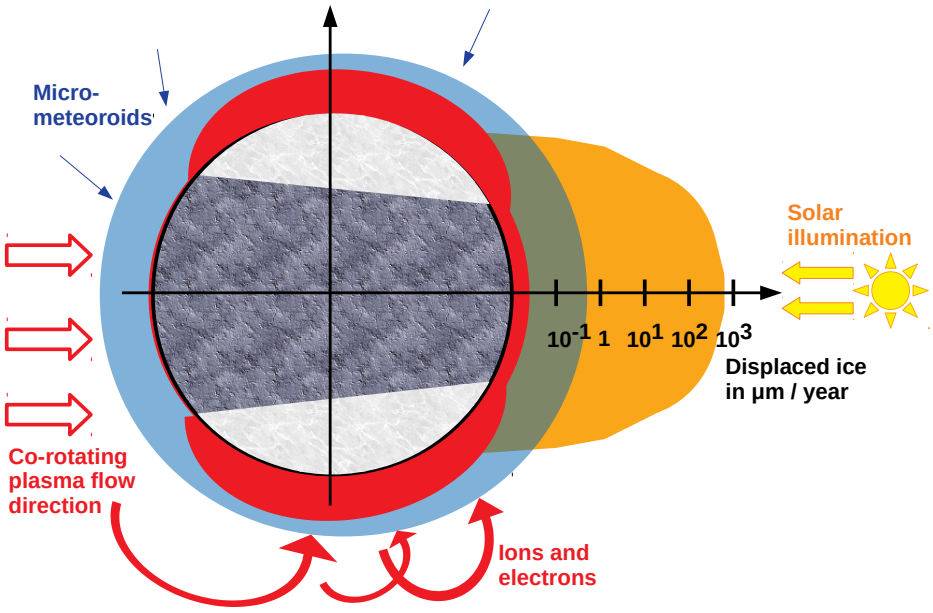

Figure 1: Sketch of water ice removal or turnover rates on Ganymede's surface in units of μm yr^{-1}. Orange shape: effect of thermal sublimation, blue: micrometeoroid impacts, red: irradiation-related rates **(dominated by ion sputtering)**. Note the logarithmic scale of the rates (going from 0.1 to 1000 μm yr^{-1}). The sketch is centred on the equatorial plane of the anti-Jovian side. Ganymede's leading hemisphere with respect to Jupiter and the Jovian plasma is on the dayside to the right. The grey band and the white pole caps symbolize the surface areas of low and high albedo.

The term "radiolysis", on the other hand, designates the chemical alteration of surface species induced by the deposited energy of the particles. The sputtered ejecta may be the original molecules of the surface (e.g., H_2O), molecule or atomic fragments (e.g., OH, O), or radiolysis products (Teolis et al., 2017; Galli et al., 2018b). The detection of O_2 (Spencer et al., 1995) and O_3 (Noll et al., 1996) in the surface, e.g., indicates radiolysis of water ice. Irradiation processes are the main topic of this chapter and are characterized in more detail in Section 3.

2.2. Thermal Sublimation

This is the surface alteration process that is easiest to quantify and understand in terms of theory and laboratory experiments. On Ganymede, thermal sublimation is most relevant at the equatorial regions, because they encounter more solar illumination and their surface is darker compared to polar regions (*see Chapters 1.5.3 by Ralf Jaumann and 2.5 by Katrin Stephan*). The surface temperatures on Ganymede range between 100 K (polar regions) and 150 K (subsolar point) (Orton et al., 1996; Ligier et al., 2019) *(see Chapter 2 for more details).*

For a given surface temperature, we can predict the sublimation rate of water ice relying on work done by Bohren and Albrecht (1998); Andreas (2007). The sublimation mass flux $S(T)$ in kg m^{-2} s^{-1} for pure water ice of temperature T calculates to:

$$S(T) = p_{sat}(T) \left(\frac{m_w}{2\pi RT} \right)^{1/2} \tag{1}$$

with R is the universal gas constant and m_w is the molecular mass of water. The saturation vapour pressure $p_{sat}(T)$ (in units of Pa) depends very strongly on temperature (in units of K) (Murphy and Koop, 2005):

$$p_{sat} = \exp\left(9.550426 - \frac{5723.265}{T} + 3.53068 \ln T - 0.00728332T\right) \tag{2}$$

Equation 2 accurately fits laboratory data over the temperature range from 110 to 273.15 K (Andreas, 2007). The corresponding sublimation rate $S(T)$ for water ice is plotted in Fig. 2.

As a consequence of Equations 1 and 2, 1 cm of porous water ice with a density of 500 kg m^{-3} is sublimated within 16 billion years if said ice layer is kept at $T = 100$ K at Ganymede's polar regions (blue dashed line in Fig. 2). The same ice layer is removed within just 16 years if $T = 150$ K (red dashed

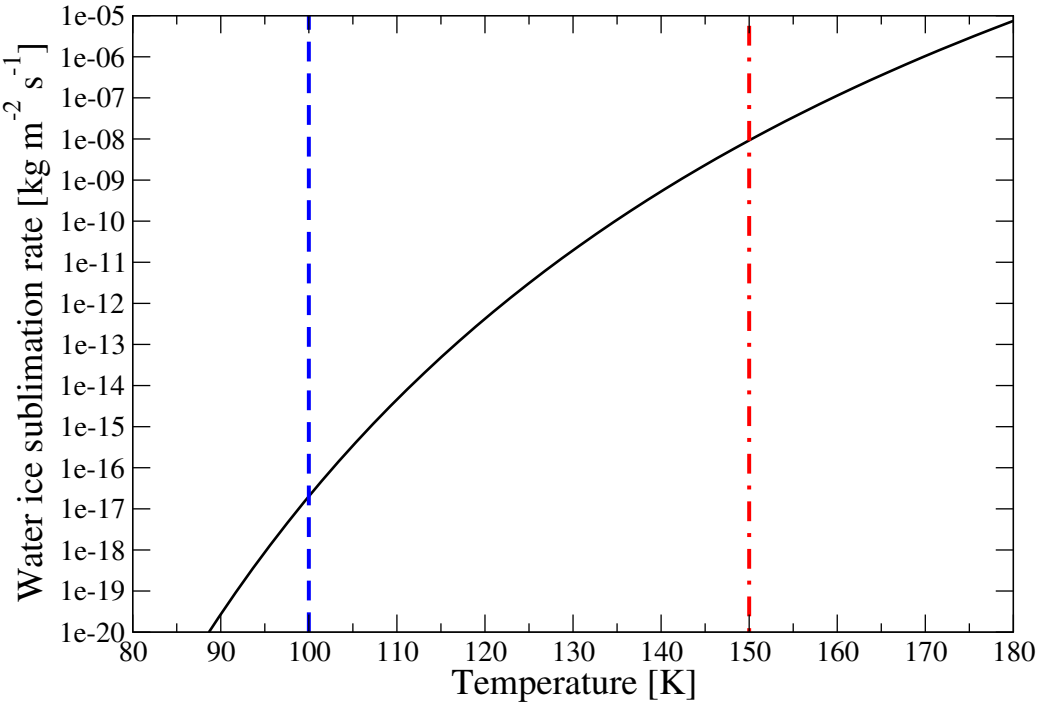

Figure 2: Water ice sublimation rate (black) as a function of temperature, from the semi-empirical formula by Murphy and Koop (2005) and Andreas (2007). Note the logarithmic scale of the sublimation rate! Typical temperatures on Ganymede's surface are depicted by the blue, dashed line (night-side and polar regions, 100 K) and by red, dashed-dotted line (subsolar region, 150 K).

dotted line in Fig. 2)! Water ice on Ganymede is thus very unstable at the dark warm regions near the equator and very stable at the colder, brighter regions. This is illustrated by the pronounced erosion peak around the equator in Fig. 1 for water ice. Non-volatile surface constituents (silicates, hydrated salts, etc.) are not much affected by thermal effects. Temperature-dependent sublimation at sun-lit regions and subsequent cold-trapping of the released water in polar regions thus may cause the differentiation into bright and dark albedo regions on the surface (see Section 4.1). **Because of the** negative feedback between water ice content and equilibrium surface temperature, this differentiation can also operate on smaller scales, leading to localized patches of pure water ice persisting in equatorial regions where the surface temperatures on top of silicate-ice mixtures do not allow for permanent water ice deposits. Indeed, surface temperature differences between two adjacent geological units can reach up to 25 K (Pappalardo et al., 2004; Stephan et al., 2020). This estimate from a geological perspective agrees with the sublimation curve in Fig. 2: Regions covered by pure water ice cannot exceed surface temperatures of 128 K, otherwise these regions would lose more than 1 m of ice within less than 1 million of years. Sublimation also leads to the formation of a transient H_2O atmosphere below a few 100 km altitudes at the equatorial regions around the subsolar point (see e.g. Marconi (2007); Turc et al. (2014); Plainaki et al. (2015) **and recent observations by Roth et al. (2021)**).

Other ices of interest for Ganymede, such as CO_2 (Mura et al., 2020) and O_2, are less stable than water ice if they were to exist in pure form on the surface (Fray and Schmitt, 2009). On the other hand, volatile oxygen-bearing species produced by radiolysis may be trapped between water ice molecules. In this form, CO_2, O_2, H_2O_2, HO_2, SO_2 and others may remain stable against sublimation until $T \approx 130...160$ K when the surrounding water ice matrix sublimates or the water ice transitions from amorphous ice to the cubic or hexagonal structure (Bar-Nun et al., 1985; Johnson et al., 2004; Bahr et al., 2001; Teolis et al., 2009; Laufer et al., 2017). O_2 molecules trapped at dangling H bonds inside the water ice may outgas to the surface via thermal desorption at somewhat lower temperatures than required for full sublimation (Johnson et al., 2019). H_2 and noble gases cannot be permanently trapped in water ice at any Ganymede surface temperatures (Bar-Nun et al., 1985).

2.3. Micrometeoroid Impacts

Micrometeoroid and meteoroid impact studies dedicated specifically to Ganymede are rare (e.g., Krüger et al. (2000); Miljkovic et al. (2012)). Micrometeoroids are expected to release all surface species non-discriminatingly into the atmosphere by impact vaporization and ejection of dust grains. The ejection yield per impactor is very high (typically 10^4 (Krüger et al., 2000)), but only a tiny fraction of the ejected grains leaves Ganymede entirely. Krüger et al. (2000) estimated, based on dust detector measurements onboard the Galileo spacecraft, that the majority of micrometeoroids hitting Ganymede's surface **are** interplanetary dust grains **(predominantly from Jupiter-family comets according to Poppe (2016))** with a total mass flux of 30 g s^{-1} at the present. With a yield of 10^4, the authors estimated that 10^2 to 10^3 kg s^{-1} of Ganymede's surface material is released from the surface. Since most material returns to the surface eventually, the main effect of micrometeoroids on the surface is that they erode and turn over the surface layers, the so-called impact-gardening. Cooper et al. (2001); Johnson et al. (2004) estimated re-surfacing rates on Ganymede of 0.3–1.2 μm yr^{-1} (≈ 0.3 μm yr^{-1} according to Krüger et al. (2000)) due to impact-gardening compared to $0.01 - 0.1$ for ion sputtering, and 0.1 μm yr^{-1} for sublimation at $T = 125$ K (see Fig. 2). This implies that impact gardening is relevant compared with the previous processes (sputtering and sublimation) for specific areas on Ganymede's surface (see summary in Section 5).

The average impact rate is about 4 times higher on the leading than on the trailing hemisphere judging from the observed crater density (Dones et al., 2009) and the dynamical evolution model by Bottke et al. (2013). Micrometeoroid impacts therefore may have contributed to the uneven distribution of H_2O-ice and the corresponding albedo differences of Ganymede's surface (see Section 4.1). One caveat is that the work by Bottke et al. (2013) addresses precipitation of dust fragments from disintegrated satellites early in the Jupiter system history rather than present-day micrometeoroid fluxes**, which are dominated by interplanetary dust (Krüger et al., 2000; Poppe, 2016). The trend of micrometeoroids preferentially impacting the leading rather than the trailing hemisphere should hold for both cases, but the precipitation from disintegrated satellites may have resulted in an early mass influx rate to Ganymede of 10^5 to 10^6 g s^{-1} during the first 40 million years after the capture of irregular satellites (Bottke et al., 2013) compared with today's 30 g s^{-1}.**

2.4. Photo-stimulated Desorption

Neglecting photo-stimulated desorption or "photosputtering" for Ganymede surface and atmosphere models is often motivated by references to Westley et al. (1995) and Johnson (1990). However, a more detailed examination by Johnson et al. (2004) for individual icy satellites indicated that the energy deposited by UV photons with sufficient energy to dissociate water ice (8×10^8 keV cm^{-2} s^{-1} with $E > 6$ eV) exceeds the average energy flux deposited by charged particles (2×10^8 keV cm^{-2} s^{-1} ions and electrons with $E > 10$ keV, (Cooper et al., 2001)) for Ganymede's equatorial regions. For the polar regions outside the closed magnetic field lines, the UV energy deposition is an order of magnitude lower than the energy flux deposited by charged particles. Neglecting photo-stimulated desorption for Ganymede surface alteration and release processes can be motivated nevertheless, but this has to include consideration of the yields for the various competing processes. Considering Lyman-alpha photons, the main constituent of the solar UV energy flux, the yield of released water molecules per photon is 0.005 to 0.01 for relevant water ice temperatures of 80 and 120 K, respectively (Westley et al., 1995). This yield is several orders of magnitude lower than the sputter yield for ions from the Jovian magnetosphere and Ganymede's ionosphere (see Section 3.2.1).

3. Irradiation Processes

The space environment of Ganymede is filled with three populations of charged particles: 1) The thermal plasma corotating with the magnetic field lines of Jupiter (Kivelson et al., 2004; Poppe et al., 2018), 2) energetic particles of the Jovian magnetosphere with tens of keV to MeV energy consisting of H^+, O^{2+}, and S^{3+} ions and electrons (Mauk et al. (2004); Allioux et al. (2013); Poppe et al. (2018); Plainaki et al. (2020a); Carnielli et al. (2020); Liuzzo et al. (2020) and *book chapter 3.1*), and 3) the ions and electrons of Ganymede's own ionosphere (mostly O_2^+ **for the ions**, see Carnielli et al. (2020) and *book chapter 3.4*). **The impacting particles penetrate Ganymede's surface at depths from hundreds of nanometers (slow ions) to meters (MeV electrons including their bremsstrahlung photon products) (Paranicas et al., 2002). In this process, particles** can directly eject surface molecules (sputtering) and also trigger chemical reactions in the ice (radiolysis). In this Section, we first characterize the particle precipitation for these surface processes (Section 3.1) and then proceed to the description

of the irradiation processes taking place on the icy and non-icy surfaces on Ganymede (Sections 3.2.1 and 3.2.2).

3.1. Particle Precipitation on the Surface

The interactions between the Jovian plasma, Ganymede's intrinsic magnetic field, and the ionosphere make it very challenging to quantifying the different particle populations and species bombarding Ganymede's surface. To compare the relative importance of particle populations, we must discern between the particle fluxes (where thermal plasma may dominate because of the higher number and density) and the deposited energy or sputtering rate or reaction rate per area, for which the energy of the particles and further energy-dependent parameters like the sputtering yield (see Section 3.2) must be taken into account. Consideration of particle precipitation at Ganymede must differentiate between the polar regions coinciding with open magnetic field lines versus the equatorial latitudes inside closed magnetic field lines and also between the leading versus the trailing hemisphere relative to the co-rotating Jovian plasma *(see book chapter 3.1)*.

The in-situ measurements of the Galileo spacecraft in the 1990s allowed to quantify the Jovian plasma environment for the first time. Based on these measurements, Cooper et al. (2001); Mauk et al. (2004) compiled energy spectra of the main ions (H^+, O^{n+}, and S^{n+}) and electrons and estimated energy fluxes on the surfaces of Europa, Ganymede, and Callisto (see Fig. 3 **for Ganymede). Cooper et al. (2001) predicted for Ganymede** that electrons were the dominant contributor in terms of deposited energy in the polar regions, whereas energetic S^{3+} and O^{2+} dominated the energy flux in equatorial regions.

Based on recent modelling efforts by (Poppe et al., 2018; Plainaki et al., 2020a; Carnielli et al., 2020) the ion precipitation on Ganymede's surface can be summarized as follows *(see book chapter 3.3.2. for more details)*: Energetic S^{3+} and O^{2+} from the Jovian magnetosphere are the dominant contributors**, among all ion populations,** in terms of deposited energy and triggered irradiation processes for most surface regions. The precipitating fluxes and sputtering rates of all energetic particle species decrease from polar regions to equatorial leading hemisphere to equatorial trailing hemisphere. This is illustrated by the map of combined ion precipitation flux in Fig. 4. The main reason for the polar equatorial dichotomy is Ganymede's dipole magnetic field, separating the surface in regions linked to open (polar regions) and regions linked to closed magnetic field lines (equatorial regions).

The relative enhancement of precipitation on the leading versus the trailing equatorial regions is caused by Jovian plasma that overtakes Ganymede and then is dragged into and heated up in the magnetic field reconnection region downstream from the satellite, i.e. above Ganymede's leading side (Poppe et al., 2018).

The extent of these spatial differences in precipitation fluxes and sputtering rates seems to be model-dependent to some extent and may also depend on the importance of the ionosphere (Poppe et al., 2018; Plainaki et al., 2020a; Carnielli et al., 2020). Carnielli et al. (2020), e.g., predict (see Fig. 5) S^{3+} to dominate among Jovian particle precipitation and the water ice sputtering rate to be rather uniformly distributed across Ganymede's surface (for G2 flyby conditions). By comparison, Poppe et al. (2018) predict that neutral sputtering is reduced by factors of 2.5 and 10 in the leading and trailing hemispheres, respectively, with respect to the polar regions. The dynamics of the entry and circulation of the Jovian energetic ions inside Ganymede's magnetosphere, the formation and extent of the ionosphere, and the morphology of the ion precipitation onto the surface determine the variability of the water release. Plainaki et al. (2020a) have studied this variability for three specific Galileo flybys.

Energetic ions can be trapped inside Ganymede's magnetic field lines *(see book chapter 3.1)*. Contrary to the Jovian energetic particles, the energy-weighted precipitation pattern of these ionospheric ions peaks in the equatorial regions of the leading hemisphere. The relative importance of ionospheric ion precipitation relative to Jovian ions is hard to quantify because of the ill constrained atmospheric densities. The contribution of ionospheric ions ranges between 10% and 70% of the total water ice release rate by all ion species (Carnielli et al., 2020).

Jupiter's electron environment was recently modelled by de Soria-Santacruz et al. (2016); Jun et al. (2019) and the resulting precipitation of energetic Jovian electrons onto Ganymede's surface has been studied by Liuzzo et al. (2020). The precipitation pattern of energetic electrons (see Fig. 6) follows basically the one seen for energetic ions (see Fig. 4), with one qualitative difference: The minimum of energetic electron precipitation in equatorial regions (within closed field line regions) occurs near the anti-Jovian point (180° W longitude), in contrast to the sub-Jovian point at 0° for the ion precipitation minimum. This difference between positively and negatively charged particles is due to the particles' opposite drift direction within Ganymede's internal field (Liuzzo et al., 2020).

Open-closed field lines boundaries shield electrons below 40 MeV from the equatorial regions, above 100 MeV electrons can hit Ganymede's surface anywhere. These equatorial electron fluxes are enhanced in the leading, sub-Jovian hemisphere (Liuzzo et al., 2020). Discussing relative contributions of particle precipitation in the polar regions, **Liuzzo et al. (2020)** find that the contribution to the number flux **(and to the energy flux)** of charged particles from energetic electrons exceeds the ion contribution by an order of magnitude and that the high-latitude regions are strongly irradiated to a depth of roughly 10 cm.

Low-energy electrons with $E \leq$ few keV from the thermal plasma have penetration depths less than a micrometer (Johnson, 1990; Hand and Carlson, 2011), and their relevance on Ganymede surface processes has so far hardly been studied. Frank et al. (1997) derived, based on Galileo flyby measurements, that electron energy fluxes between 70 eV and 4.5 keV into the polar regions amounted to roughly 10^9 keV cm^{-2} s^{-1} at the time of flyby. This is 5 times less than the total energy deposited by energetic ions and electrons (Cooper et al., 2001). Neglecting low-energy (below roughly 10 keV) electron precipitation thus seems to be acceptable to first order approximation, but future plasma models should cover this aspect, too, and also assess the importance of ionospheric electrons.

Now that we have set the scene with the plasma and energetic particle precipitation maps, we will discuss the reactions triggered by this precipitation.

3.2. Description of Irradiation Processes

Beside regions rich in water ice, Ganymede's surface also shows areas covered with hydrated sulphuric acid ($H_2SO_4 * nH_2O$), salts, and an unidentified darkening agent hypothesized to contain hydrated silicates (Ligier et al., 2019). A simplified table of chemical abundances based on the near-infrared imaging spectrometer observations by Ligier et al. (2019) is shown in Tab. 2 *(Also refer to book chapters 1.5.3 and 2.5)*. We therefore will describe the irradiation processes known from theory and laboratory experiments distinguishing between irradiation of water ice (or other condensed gases) and non-icy target material of interest for Ganymede (hydrated sulphuric acid, salts, and potentially hydrated silicates).

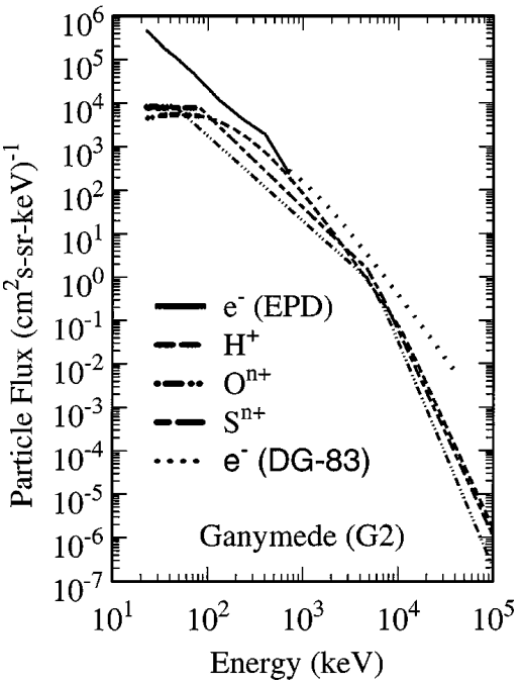

Figure 3: Energy spectra of the major energetic particle species in Jupiter's magnetosphere upstream of Ganymede, derived from Galileo measurements during the G2 flyby. Figure from Cooper et al. (2001).

Table 2: Relative chemical abundances presumed for polar and equatorial surface regions, based on Ligier et al. (2019).

	Water ice	Dark material	Sulphuric acid hydrate	Sulfates	Chlorinated salts
Equatorial	0.15 ... 0.24	0.55 ... 0.70	0.04 ... 0.10	0.03 ... 0.08	0.03 ... 0.08
Polar	0.40 ... 0.48	0.30	0.16	0.03	0.03 ... 0.11

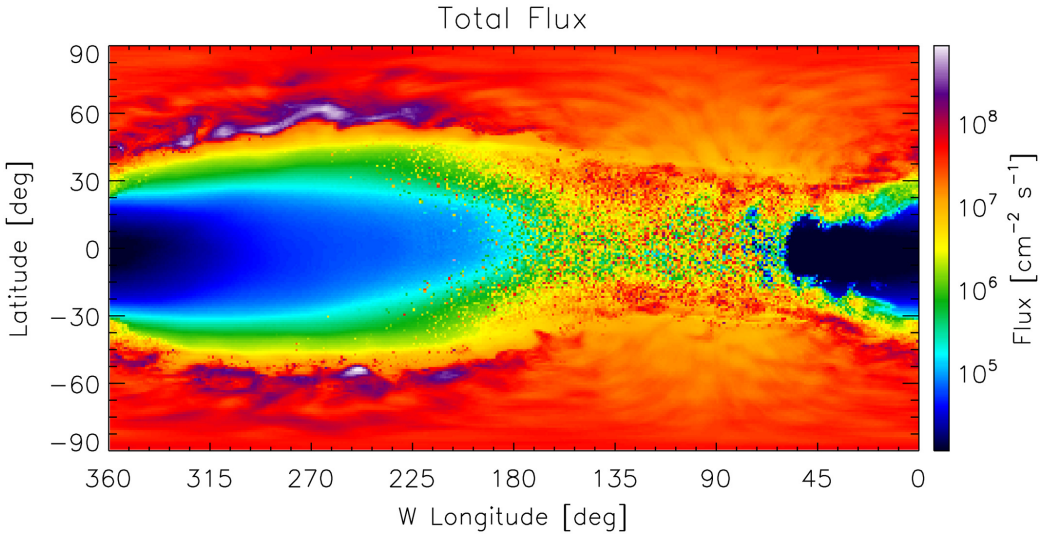

Figure 4: Total ion precipitation flux onto Ganymede's surface, summed over all ion species and energies, representative of G8 configurations when Ganymede was inside the Jovian plasma sheet. Leading hemisphere is centred at 90° W. Figure from Poppe et al. (2018).

3.2.1. Irradiation of Water Ice

Irradiation of water ice by charged particles is an important source process for the chemical and physical alteration of the surface and for the generation of Ganymede's atmosphere (*see details in chapter 3.3*). Bearing in mind the wide variety of particles precipitating onto Ganymede, we attempt a general distinction before discussing the details for the different types of irradiation processes: Energetic electrons dominate radiolysis rates of water molecules below the uppermost ice layers (depths of micrometers to centimetres), whereas energetic ions dominate the total mass loss rate from the icy surface. Finally, thermal plasma may be relevant because the implanted ions provide additional building blocks for chemical reactions in the ice.

Electron Irradiation:

At ice temperatures relevant to Ganymede, **most water molecules that are radiolyzed** leave the ice via the reaction $H_2O \rightarrow H_2 + \frac{1}{2}\ O_2$ once irradiation has reached saturation levels (Petrik et al., 2006; Abdulgalil et al., 2017; Galli et al., 2018b). At much colder temperatures ($\simeq$ 10 K instead of $\simeq$ 100 K), radiolysis would produce and release more H_2O_2 than O_2 (Zheng et al., 2006). **Little H_2O, compared with H_2 and O_2, is released by elec-**

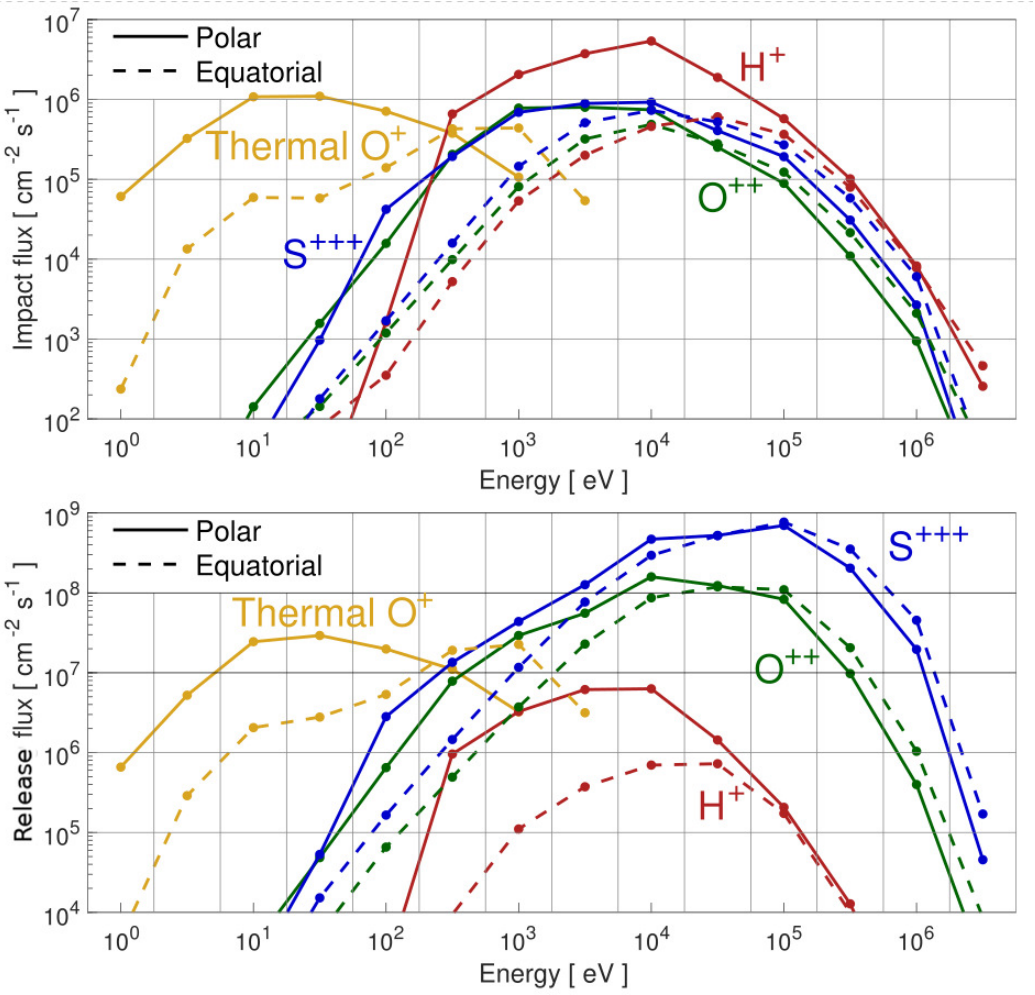

Figure 5: Impact (top) and release (bottom) fluxes as a function of impact energy for different Jovian ion species: O^+ from the thermal population (gold), energetic H^+ (red), energetic O^{2+} (green) and energetic S^{3+} (blue). The solid curves show values in the region of open magnetic field lines (north and south polar regions combined), while the dashed lines show values in the region of closed magnetic field lines. Figure adapted from Carnielli et al. (2020).

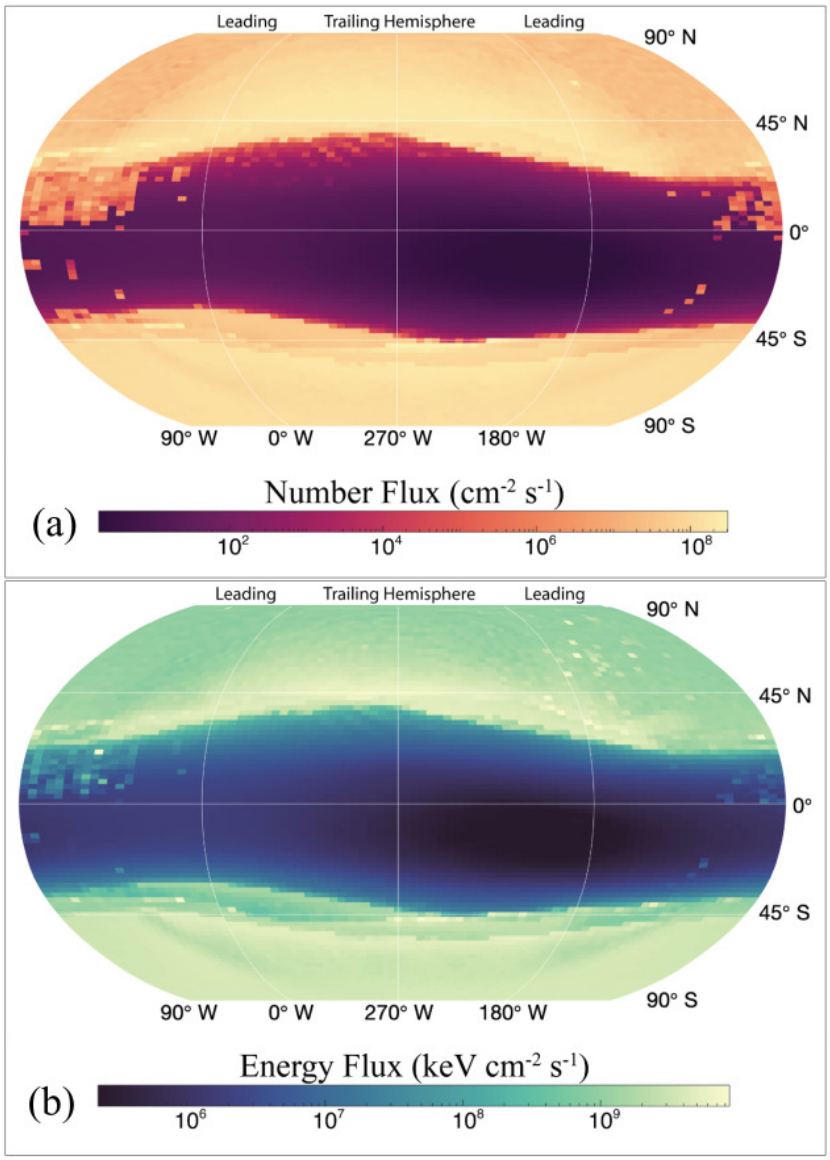

Figure 6: Energetic electron (a) number and (b) energy flux deposited onto Ganymede's surface averaged over a full Jovian synodic period. Figure taken from Liuzzo et al. (2020).

tron irradiation at temperatures relevant for Ganymede according to Abdulgalil et al. (2017); Teolis et al. (2017); Galli et al. (2018b) whereas the ratio of released H_2O/O_2 reaches unity at such temperatures according to Davis et al. (2021). Some O_2 on the order of 1% **with respect to** H_2O (Grieves and Orlando, 2005; Galli et al., 2021) and H_2O_2 (0.04% and 0.006% by number relative to water at 80 K and 120 K, respectively (Hand and Carlson, 2011)) can remain trapped in irradiated water ice provided the temperature remains below 150 K (Zheng et al., 2006). H_2 is too volatile to be retained in the ice at Ganymede surface temperatures (Bar-Nun et al., 1985; Galli et al., 2021). Once O_2 builds up in the ice, electron irradiation will also form O_3 from O_2 (Sivaraman et al., 2007) but so far, to our knowledge, no O_3 was directly produced from irradiating water ice with electrons in laboratory.

Electron irradiation can also amorphize crystalline water ice (Baragiola et al., 2003; Loeffler et al., 2020), reduce micro-porosity (Behr et al., 2020), and lead to sintering (Howett et al., 2011, 2012; Ferrari and Lucas, 2016; Nordheim et al., 2017; Schaible et al., 2017). The first effect has been conjectured to be responsible for the observed amorphous water ice in the polar regions (Hansen and McCord, 2004; Liuzzo et al., 2020).

The total mass loss rate due to radiolysis and subsequent release of H_2, O_2 etc. is sometimes described as sputter yield $Y(E)$ due to electron irradiation. This value is usually determined by measuring the electron-induced mass loss rate of ice deposited on a microbalance. For thermal and low-energy electrons, theory and experiments agree Orlando and Sieger (2003); Teolis et al. (2017); Galli et al. (2018b); Meier and Loeffler (2020) that this yield increases with energy to reach a maximum or plateau around 1 keV. For higher energies, two conflicting interpretations of experiments exist: Whereas consideration of electron stopping power and microbalance measurements with compact ice films at temperatures of 60 K indicate that $Y(E)$ decreases with energy above 1 keV (the solid curve in the top panel of Fig. 8), experiments with thick layers of porous water ice at 100 K indicated that the sputter yield remains roughly constant from 1 to 10 keV electron energy (Galli et al., 2018b). Moreover, the absolute sputter yields predicted or measured by Teolis et al. (2017); Galli et al. (2018b); Meier and Loeffler (2020) only agree within one order of magnitude. These open questions about the yield are maybe not crucial for our understanding of Ganymede's surface: The different studies do not disagree regarding the radiolysis rates triggered inside the irradiated ice and all atmospheric source rates (with possible exceptions

for H_2 and O_2) are dominated by energetic ions with their sputter yields $Y \approx 100 \ldots 1000$ (Vorburger and Wurz, 2018).

The penetration depth of electrons in water ice increases with energy in a way that can be approximated by a power law (Johnson, 1990; Hand and Carlson, 2011)

$$d \approx R_0 E^{\alpha} \tag{3}$$

with E the electron energy in units of keV, $\alpha = 1.76$, and the depth $R_0 = 46$ nm for targets with density $\rho = 1$ g cm^{-3} at 1 keV. This implies a penetration depth of 1 cm for a 1 MeV electron**, but such energetic electrons can cause radiolysis down to depths of ~ 1 m because of the bremsstrahlung photons produced inside the ice (Paranicas et al., 2002).**

Ion Irradiation:

Impacting ions directly eject H_2O molecules because of the larger energy deposition per unit path length of ions compared to electrons. But ions can initiate radiolysis, too, leading to chemical alteration of the ice and ejection of the newly formed species. Irradiation of water ice with H, O, and S ions can therefore result in the formation and/or ejection of H_2O, H_2, O_2, H_2O_2, O_3 but the exact ratios in the irradiated ice and the ejecta are difficult to quantify and depend on many different parameters including at least ion energy, ion species, and ice temperatures (Haring et al., 1984; Cooper et al., 2005; Boduch et al., 2016).

Most results of ice sputtering experiments before 2010 were collected by Johnson and Liu (2010) in an online database. The impacting species include H, noble gases up to Xe, C, N, O, and F, with energies ranging from roughly 1 keV to 25 MeV. More recently, Muntean et al. (2016); Galli et al. (2017) showed in laboratory experiments that singly and doubly charged ions produced the same sputtering yield on water ice. The so-called potential sputtering by multiply charged ions (Aumayr and Winter, 2004) thus seems to be irrelevant for Ganymede's surface, in addition the charge state of ions usually does not exceed 3 (see previous section). On the other hand, Galli et al. (2017) found that O_2^+ molecular ions show a factor of 2 higher sputter yield than expected from O^+ ions of the same total kinetic energy. Finally, Galli et al. (2018a) measured sulphur sputtering yields on water ice for the first time under laboratory conditions.

For ion energies below 1 keV, the sputtering yield of ions in water ice can be described by a cascade of elastic collisions, whereas at higher energies, the

so-called electronic sputtering dominates. Famá et al. (2008) derived a semi-empirical formula for the sputtering yield for the sum of both contributions, based on laboratory experiments with thin water ice films:

$$Y(E, m_1, Z_1, \theta, T) = \frac{1}{U_0}\left(\frac{3}{4\pi^2 C_0}\alpha S_n + \eta S_e^2\right)\left(1 + \frac{Y_1}{Y_0}\exp\left(-\frac{E_a}{kT}\right)\right)\cos^{-f}(\theta). \quad (4)$$

Equation 4 quantifies the sputtering yield as a sum of elastic and electronic sputtering, described by the nuclear stopping power S_n and the electronic stopping power S_e. The sputtering yield depends on energy E, mass of impactor m_1, atomic number of impactor Z_1, the incidence angle θ from the surface normal, and temperature T. For U_0, the sublimation energy of water (0.45 eV) is assumed, $C_0 = 1.3$ Å^2, $E_a = 0.06$ eV, and $Y_1/Y_0 = 220$ are constants. The temperature-independent fraction in Equation 4 is due to the direct ejection of H_2O molecules. The temperature-dependent term with the activation energy E_a becomes dominant above $T = 120$ K and is due to the release of H_2 and O_2 (Johnson et al., 2004; Famá et al., 2008; Teolis et al., 2009). Water radicals inside the irradiated ice react to H_2 and O_2 (Cassidy et al., 2010; Galli et al., 2018b) and are then released by ion sputtering (O_2) or diffusion (H_2).

Cassidy et al. (2013) examined the data compiled by Johnson and Liu (2010) and found that the semi-empirical sputtering Equation 4 fits data well for energies below 100 keV. At higher energies, the formula by Johnson et al. (2009) for electronic sputtering is more accurate. This is illustrated in Fig. 7 for the three most common ion species H^+, O^+, and S^+ including some of the data from laboratory experiments. The yield curves peak in the energy range between 10 keV and 10 MeV. This fact, together with the yields (of the order of 10–1000 for 1 keV – 1 MeV O and S ions that form the bulk of energetic ions precipitating onto Ganymede, Fig. 5), explains why sputtering by energetic O and S dominates the surface erosion rate among all irradiation processes.

Experiments under laboratory conditions also showed that most of the removed water ice is ejected as water molecules but a fraction of the water ice is radiolysed by the ions into O_2, H_2, H_2O_2, and O_3 (Bahr et al., 2001; Teolis et al., 2006, 2009). The O_2/H_2O ratio of the released particles is not a fixed fraction of the total sputtering yield, it depends both on the energy of the impactor and the temperature of the ice. Below 100 K, the O_2 production upon Ar irradiation was found to be negligible, whereas some

H_2O_2 was produced. At ice temperatures above 100 K, H_2O_2 production was suppressed whereas the O_2/H_2O ratio increased with temperature (Teolis et al., 2009). The relative contribution of O_2 to the total mass released from the ice was found to be highest (roughly 20%) for ion energies around 10 keV (Teolis et al., 2017). The yields of H_2O and O_2 from water ice regolith, in the absence of thermal effect, are shown in Fig. 8 for all relevant impactors.

The penetration depths of ions increase with energy and decrease with ion mass. Sulphur and oxygen ions with energies between 10 and 100 keV reach typical ranges of tens to hundreds of nm in water ice, 70 keV S^+ ions, e.g., reach about 150 nm depth on average according to SRIM simulations (Galli et al., 2018a). Electrons of the same energy penetrate 500 times deeper in ice before being stopped (see Eq. 3).

Finally, we also must consider that the impacting ions remain implanted in the water ice. Energetic sulphur ions implanted in 80 K water ice form hydrated sulphuric acid H_2SO_4 at a high yield of 0.65 ± 0.1 molecules/ion under laboratory conditions (Strazzulla et al., 2007). The total flux of 10^6 cm^{-2} s^{-1} sulphur ions (see Fig. 5) thus results in the production rate of roughly 10^6 H_2SO_4 molecules cm^{-2} s^{-1} in the polar regions on Ganymede. As a result, the distribution of sulphur-bearing species on Ganymede's surface reflects the availability of Jovian sulphur ions and water ice (see Section 4.2).

3.2.2. Irradiation of Non-watery Species

Both the chemical composition of the non-icy compounds (hydrated sulphuric acids, salts, silicates, etc.) and the interaction of these chemical compounds with energetic electrons and ions is far less well known than for water ice targets.

The chemical reaction pathways and subsequent release processes of irradiated sulphuric acid or other **sulphur-bearing** compounds in water ice have been investigated by Carlson et al. (1999, 2002); Moore et al. (2007); Loeffler et al. (2011); Loeffler and Hudson (2012). In principle, ions and UV photons can decompose H_2SO_4 in the uppermost layer, but the high radiation stability of hydrated H_2SO_4 at temperatures $\simeq$ 100 K or higher means H_2SO_4 hydrates are more abundant than SO_2 and polymerized sulphur (Carlson et al., 1999; Loeffler and Hudson, 2012). Loeffler et al. (2011) **observed for the 120–130 K temperature range that the ices become more stable with increasing hydration state of the sulphuric acid, which suggests that hydrates such as hemihexa-hydrate (H_2SO_4*6.5H_2O) and octahydrate (H_2SO_4*8H_2O) are stable on geological timescales**. For

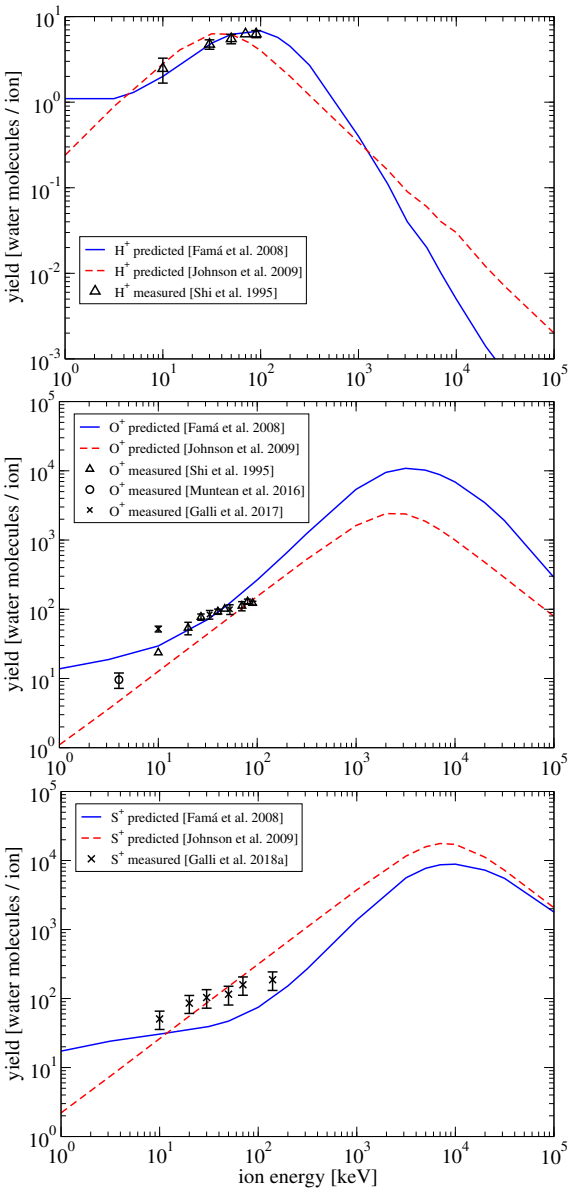

Figure 7: Ion sputtering yields for an ice temperature of 100 K and an incidence angle of 45° including semi-empirical formulae by Famá et al. (2008) (blue solid curves) and by Johnson et al. (2009) (red dashed curves) and some experiment results (Shi et al. (1995); Muntean et al. (2016); Galli et al. (2017, 2018b), black symbols) for H^+ (top panel), O^+ (middle) and S^+ (bottom).

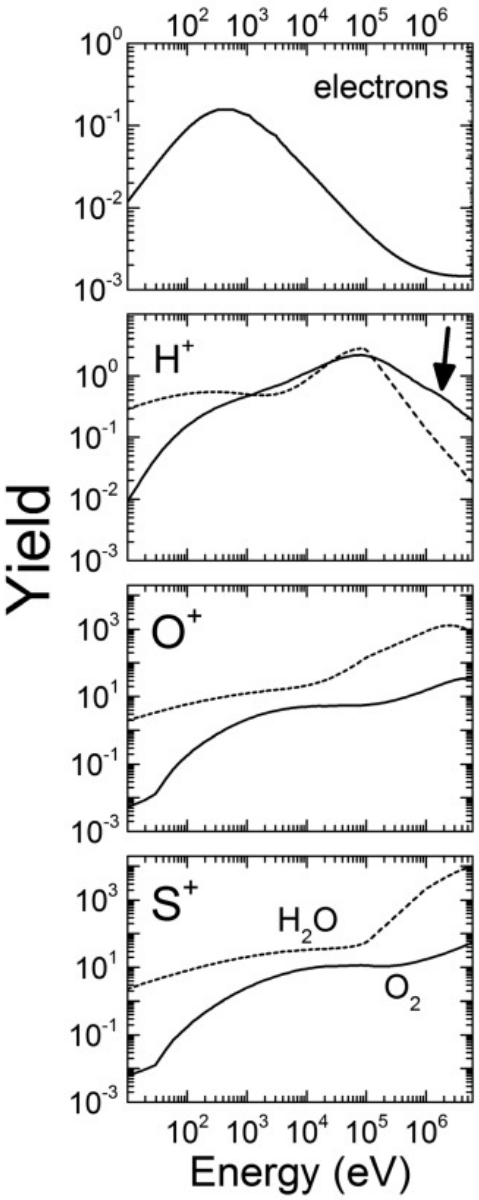

Figure 8: Predicted O_2 radiolysis yield (solid lines) and H_2O sputtering yield (dashed lines) in molecules per projectile, from a water ice regolith versus energy E in the low-temperature limit ($\leq$ 80 K and $\leq$ 130 K for O_2 and H_2O, respectively). Arrow: model may be overestimating O_2 yields for high-energy H^+ ions. Reprint from Teolis et al. (2017).

the irradiation of heavily hydrated sulphuric acid on Ganymede's surface at temperatures 100–150 K (see Section 2.2), we thus can assume that any potential new **sulphur-bearing** radiolysis product recombines to H_2SO_4*$8H_2O$ or a similar hydrate and remains stable on geological timescales. The chemical composition of ejecta from irradiated hydrated sulphuric acid is unknown: Based on ion sputtering experiments of H_2O ice, most ejecta should be entire H_2SO_4 molecules. However, ion irradiation of H_2SO_4 ices by MeV ions is able to produce also the radiolysis products SO_2, H_2O, S_2O_3 and H_3O judging from reflectance spectra of the irradiated ice (Loeffler et al., 2011). If we assume that hydrated H_2SO_4 qualitatively behaves like H_2O ice (both are isolating condensed gases) upon irradiation, the ratio of ejected radiolyzed products to parent molecule abundances should follow Fig. 8 for water ice: A large fraction ($\leq 90\%$) of sputtered H_2SO_4 molecules would be ejected as H_2SO_4, and only the remaining 10% would leave the ice as a combination of, e.g., $SO_2 + H_2O + \frac{1}{2}\ O_2$ but the relative abundance among alternative pathways remains unknown. Not even the sputtering yield of H_2SO_4, unhydrated or hydrated, has ever been determined in laboratory experiments to our knowledge.

Regarding the irradiation of hydrated salts, our knowledge is even more limited. Only a few studies have been published and the majority of them lacks experimental data and is usually directed at the specific case of Europa's surface: Zolotov and Shock (2001); Brown and Hand (2013); McCord et al. (2001). Even the total sputtering yield of hydrated salts is unknown. Existing simulations may be of limited use to close this knowledge gap: the commonly used sputtering simulation SRIM (Ziegler et al., 2008) and its more comprehensive version SDTrimSP (Mutzke et al., 2009), e.g., cannot simulate electronic sputtering nor the hydrate crystal structure. For anhydrous Na_2SO_4, sputtering experiments by Wiens et al. (1997) showed that the molecule usually fragments (the dominant Na-bearing species simply being the Na-atom) and the sputtering yield was akin to a metal or a silicate, i.e. $Y \approx 0.1$ instead of the $Y \approx 100 \ldots 1000$ for energetic ions irradiating H_2O or SO_2 ices (Johnson et al., 1984). McCord et al. (2001) reported that electron irradiation of anhydrous or hydrated epsomite released SO_2 as the only detectable species. In particular, the authors did not see O_2 nor H_2. Hydrated salts thus should not be treated as salts plus independent water for radiolysis. Ion irradiation experiments with hydrated salts have not been performed to the best of our knowledge. For future models and interpretation of Ganymede surface and atmosphere observations, more theoretical studies

and laboratory experiments are required to study the sputtering yields and space weathering effects of hydrated sulphuric acid, hydrated salts, and possibly hydrated silicates (if they indeed constitute the darkening agent) at conditions relevant for Ganymede's surface.

4. Surface Features Created by the Space Environment

To understand some characteristics of Ganymede's surface, we may have to refer to all of the space environment interaction processes listed at the beginning of this chapter. Here, we discuss three surface characteristics: the dark-bright albedo differences, the distribution of sulphur-bearing species, and the presence of oxygen and ozone. *The reader is also referred to book chapters 1.5.3 by Jaumann, 2.2 by Pappalardo, and 2.5 by Stephan.*

4.1. The Dark-Bright Albedo Differences

One striking characteristic of Ganymede's surface is the differentiation into bright icy and dark ice-poor regions (see upper panel in Fig. 9). This dark-bright dichotomy is most pronounced between the equatorial regions depleted of water ice and the polar ice-rich regions (Ligier et al., 2019; Mura et al., 2020). In addition, there is a less conspicuous longitudinal pattern in the surface albedo: The trailing hemisphere (180° to 360° W longitude, left part of the map) is darker on average than the leading hemisphere (Khurana et al., 2007). The nature and origin of the darkening agent concentrated on the trailing hemisphere is not known exactly, Bottke et al. (2013); Ligier et al. (2019), e.g., have proposed carbonaceous chondrite-like material or hydrated silicates. The dark material may represent the dusty remains of disintegrated smaller satellites from the early ages of the Jupiter system (Bottke et al., 2013). The authors argued that Ganymede's surface can be characterized as relatively old regions of dark terrains and younger cross-cutting lanes of bright typically grooved terrain (Bottke et al., 2013; Pappalardo et al., 2004).

Researchers have been investigating mainly two processes to explain the dark-bright dichotomy: thermal sublimation of water ice and Ganymede's magnetic field concentrating Jovian plasma precipitation to the polar regions (see e.g. Spencer (1987); Khurana et al. (2007)). Generally, the water ice abundance and surface albedo correlate with the precipitation rates of energetic ions and electrons: from equatorial trailing to equatorial leading to polar regions in ascending order (see Section 3.1). Khurana et al. (2007)

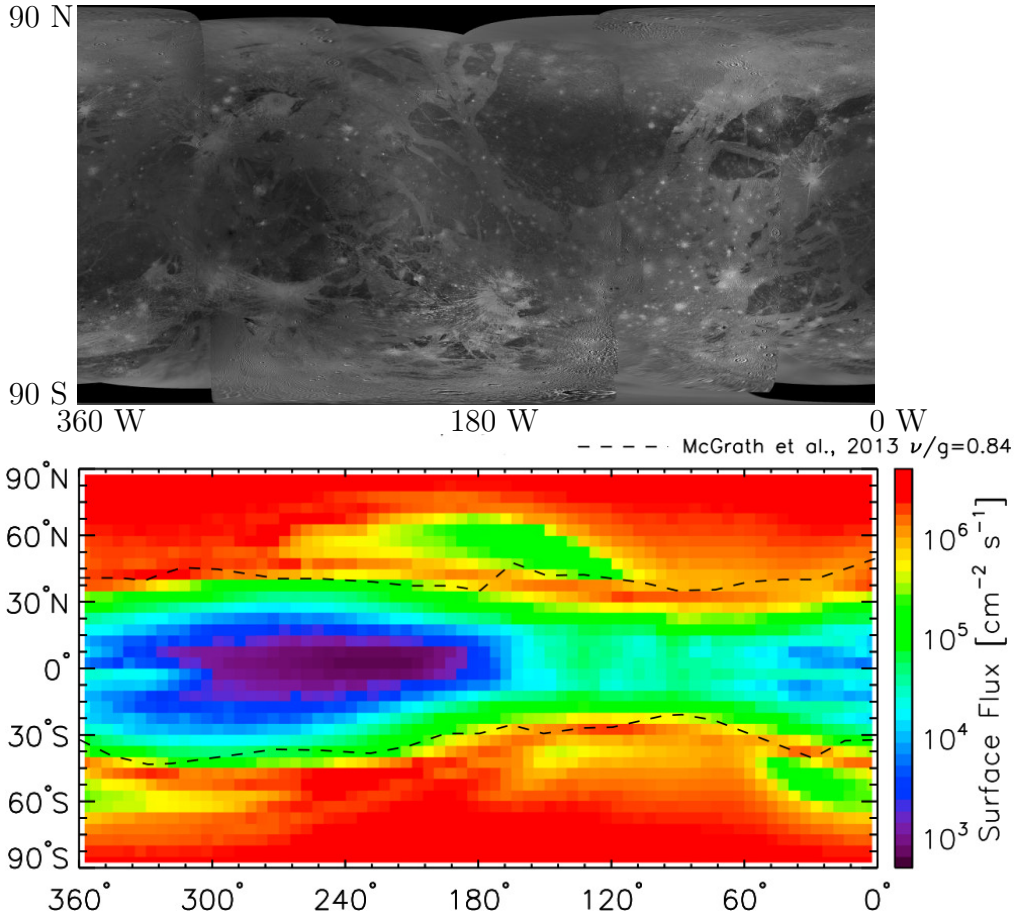

Figure 9: Upper panel: Global mosaic of Ganymede using the best image quality and moderate resolution coverage supplied by Galileo Solid-State Imaging (SSI) and Voyager 1 and 2. The left hemisphere from 360° W to 180° W is the trailing hemisphere, the right half is the leading hemisphere. Image credits: USGS Astrogeology Science Center, Batson (1984). Lower panel: Total flux of precipitating energetic ions to the surface of Ganymede from the model by Fatemi et al. (2016). The dashed lines are the violet-to-green ratio of 0.84 from the composite image of Ganymede's surface by Khurana et al. (2007) showing the approximate boundaries of Ganymede's bright polar caps and dark low latitudes.

argued that reconnection of field lines allows for the redistribution of sputter-induced water ice at low latitudes on the leading hemisphere and Fatemi et al. (2016) found a good correlation between the global surface albedo and the precipitation of Jovian energetic ions, which is organized by Ganymede's magnetic field lines. This is illustrated in the lower panel of Fig. 9.

While irradiation processes are important for Ganymede's surface chemistry and erosion rates, they are likely insufficient to create the albedo dichotomy on their own. First, from the comparison of different precipitation models of Jovian and ionospheric ions (see Section 3.1) it is not clear if ion precipitation results in energy flux depositions or ice sputtering rates orders of magnitudes stronger in polar regions compared to equatorial regions (see Fig. 5). Considerations may also have to include electron precipitation to obtain precipitation patterns strongly correlating with surface albedo ((Liuzzo et al., 2020), Fig. 6). Second, the actual surface process of how impacting ions would cause a brightening is unclear: Chemical reactions in water ice triggered by ions (sulphur ions in particular) rather deplete the water ice abundance to form other molecules. On Ganymede's neighbour Europa, the water ice-poor equatorial region (darker and yellowish, dominated by hydrated sulphuric acid and other hydrates) correlates with the **maximum** of ion precipitation, which occurs on the trailing hemisphere in the case of Europa (McEwen, 1986; Carlson et al., 1999). However, on Ganymede, the equatorial region most depleted of water ice and highest in abundance of the darkening agent coincides with the **minimum** of ion precipitation on the trailing hemisphere (Ligier et al., 2019). Ion-induced sputtering also does not lead to a local increase of icy material per se because the relevant sputter yields for water ice are orders of magnitude higher than those for non-ice species (see Section 3.2.1). Penetrating radiation (in particular due to energetic electrons), on the other hand, could brighten the surface by producing light scattering defects in water ice to a lasting effect in polar regions, whereas in warmer regions above 100 K such radiation-induced defects are annealed rapidly (Johnson, 1997).

Beside these possible explanations related to irradiation, one should keep in mind (Section 2) that there are two additional interaction processes that regionally may rival or exceed irradiation in terms of erosion rates: sublimation and impact-gardening. The spatial distribution of these processes must be compared to the particle precipitation patterns. Sublimation via its temperature-dependence produces a strong latitudinal gradient, with the erosion rate of water ice highest in the ice-poor equatorial regions. Since the

water ice sublimation rates there exceed the water ice loss rates by any other process at any region by orders of magnitude, the thermal gradient must be the main reason for the latitudinal gradient of water ice abundances. As a further argument for thermal effects, Ganymede and Callisto show similar latitudinal gradients of ice grain sizes and a dichotomy between bright polar and dark equatorial latitudes despite Callisto not possessing an intrinsic magnetic field (Stephan et al., 2020). Plainaki et al. (2020a) argued that a sputtering-assisted sublimation mechanism can explain why the trailing hemisphere low-latitude regions are darker and more depleted in H_2O ice than the leading equatorial region (Ligier et al., 2019). A clear attribution of space environment processes to surface properties becomes even more difficult when we also take into account micrometeoroid bombardment: It is expected to concentrate on the leading hemisphere (Bottke et al., 2013), too, thus coinciding with the equatorial gradient of particle precipitation. The gradient of albedo and ice-content between the leading and trailing hemisphere may be caused by a combination of meteoroid impact gardening and ionospheric precipitation (Ligier et al., 2019), in analogy to what McEwen (1986) proposed for Europa's surface.

4.2. Sulphur-bearing Species

The distribution of sulphur-bearing species looks like a well-understood phenomenon compared to the dark-bright differences. **It is known (Fatemi et al., 2016; Poppe et al., 2018; Ligier et al., 2019; Plainaki et al., 2020a; Carnielli et al., 2020) that hardly any sulphur-bearing material is visible** in equatorial trailing regions where sulphur ion precipitation is lowest, sulfates exist in equatorial leading hemisphere where precipitation is substantial and water ice is depleted because of high temperatures, and sulphuric acid hydrates (but not sulfates) are abundant in polar regions where precipitation fluxes are high and water ice is abundant because of the low temperatures.

While the occurrence of sulfates correlates with geomorphology (sulci) (Ligier et al., 2019) and thus might be related to an endogenic origin from the ocean *(see Chapter 2.7)*, the hydrated sulphuric acid is most likely exogenic. The average abundance of hydrated sulphuric acid increases from equatorial trailing to equatorial leading to polar regions from 4% to 10% to 16%, respectively ((Ligier et al., 2019) and Table 2). This correlation with precipitation fluxes of energetic sulphur ions indicates that the sulphur-bearing species are the products of impacting S ions with the water ice, in

a similar way as postulated for the trailing hemisphere of Europa (McEwen, 1986; Carlson et al., 1999, 2002; Loeffler et al., 2011). Recent simulations by Plainaki et al. (2020a) of O^{2+} and S^{3+} ion precipitation fluxes agree with Ligier et al. (2019) who inferred the likely presence of sulphuric acid hydrate by matching the obtained spectra with a limited number of reference spectra.

The inferred abundances of sulphuric acid hydrates are consistent with ion fluxes and production rates known from experiments (see Section 3.2.1): Given a production rate of 10^6 cm^{-2} s^{-1} H_2SO_4, 10% of H_2O molecules in an initially pure water ice surface are replaced by H_2SO_4 within 100 million years, which is compatible with typical surface ages of Ganymede *(see Chapter 2.3)*.

4.3. Oxygen and Ozone at the Surface

The observed absorption lines of solid O_2 and O_3 in Ganymede's surface spectrum are usually taken as direct evidence of irradiation processes on the icy surface (Spencer et al., 1995; Calvin et al., 1996; Orlando and Sieger, 2003). The original detection of solid O_2 was reported based on absorption lines in the visible range reflectance spectrum at 577 and 627 nm (Spencer et al., 1995). This discovery came as a surprise because O_2 ice would sublimate immediately at Ganymede surface temperatures (Calvin et al., 1996). Subsequent laboratory experiments demonstrated that O_2 created by radiolysis in amorphous or crystalline water ice can be retained at temperatures close to Ganymede's dayside temperatures (Grieves and Orlando, 2005; Loeffler et al., 2006; Zheng et al., 2006; Galli et al., 2021). The O_2 abundance was inferred to $0.1 \ldots 1\%$ by volume relative to H_2O and the O_2 densities appear similar to the liquid or solid γ-phase (Calvin et al., 1996). The O_2 band depths were found to be strongest at low latitudes on Ganymede's trailing side (Calvin et al., 1997). Absorption bands of solid O_2 were observed also on Europa's and Callisto's surfaces, albeit with a shallower absorption depth implying a O_2/H_2O ratio of the order of 0.1% (Spencer and Calvin, 2002).

On the trailing hemisphere of Ganymede, also O_3 was identified via the detection of the absorption band at 260 nm with the Hubble Space Telescope (Noll et al., 1996). The authors estimated a number density ratio of $[O_3]/[O_2] \approx 10^{-4}$ to 10^{-3} in Ganymede's surface. Ozone can indeed be formed efficiently under laboratory conditions when water ice is irradiated with heavy ions at ice temperatures exceeding 120 K provided water ice keeps recondensating onto the surface during the experiment (Teolis et al., 2006).

O_3 can also be formed by irradiation of an H_2O-O_2 ice mixture with electrons (Jones et al., 2014).

In contrast to Europa (Carlson et al., 1999), H_2O_2 absorption lines so far were not discovered in Ganymede's surface reflectance spectra. This can be attributed to Ganymede's surface temperatures because the H_2O_2 radiolysis production in water ice warmer than 100 K is known to become inefficient for electron and ion irradiation (Teolis et al., 2009; Hand and Carlson, 2011).

The O_2 and O_3 on Ganymede's surface cannot be a leftover from the creation time of Ganymede given today's high temperatures and the temperatures immediately after formation *(see Chapter 1.2)*. The explanation of a secondary creation via irradiation of water ice is also plausible because the creation of O_2 and O_3 by radiolysis has been demonstrated under laboratory conditions. The spatial distribution of the O_2 and O_3, however, poses a puzzle: Spencer et al. (1995); Calvin et al. (1996) argued that the concentration of the oxygen on Ganymede's trailing side suggests that it is generated by magnetospheric bombardment. There is a serious flaw in this argument as we know now. The equatorial trailing side is the region with the **lowest** particle precipitation fluxes (see Section 3.1). This was not known or fully understood in the years 1995–1997 as the discovery of Ganymede's magnetic field was reported only in 1996 (*see Chapter 3.1*). With the current knowledge of Jovian magnetosphere and particle precipitation we must reconcile the fact that the O_2 absorption bands seen on Ganymede's surface anti-correlate with irradiation levels (Bahr et al., 2001).

Moreover, the exact enriching and storage process of dense-phase O_2 in water ice after radiolysis was unclear at the time of discovery (Calvin et al., 1997) and remains so to this day. (Calvin et al., 1996) favoured defect trapping or adsorption as the likely means to obtain the O_2 absorption lines, whereas Johnson and Jesser (1997) favoured gas-filled O_2 bubbles in the ice. Vidal et al. (1997), in turn, suggested that the O_2 molecules dissolve in the ice rather than aggregate in clusters or bubbles at Ganymede's surface temperatures. This theory was contradicted by subsequent observations finding the dense-phase or dimer oxygen form predominantly in equatorial and mid-latitude regions rather than in polar regions (Calvin et al., 1997). The abundance of oxygen appeared more dependent on latitude and longitude constraints than surface albedo. Calvin et al. (1997) thus argued that defect trapping is a more plausible process than physical adsorption to explain the solid O_2 absorption lines. In the experiment by Bahr et al. (2001) with energetic proton irradiation there was no indication of radiolytic O_2 bubbles as

the source of the absorption bands of condensed O_2.

Finally, we must keep in mind that the O_2 absorption signal not only anti-correlates with particle precipitation fluxes, but also anti-correlates with water ice abundance: At latitudes below 45°, the water ice abundance (mostly in crystalline form) makes up only about 20% (Ligier et al., 2019). The temperature-dependence of the O_2 production rates in water ice (Teolis et al., 2009) might be more important than the adverse trends of water ice availability and irradiation doses, but the real explanation for the unexpected spatial distribution is currently unknown.

5. Summary

This chapter has introduced all surface interaction processes at Ganymede. We have seen that irradiation, thermal sublimation, and micrometeoroid impacts can be relevant for different specific surface areas and surface alteration processes. In terms of water erosion or turnover rates, sublimation dominates in the warm region, and micrometeoroid impacts probably are generally more important than irradiation processes. The ions and electrons from the Jovian environment and the ionosphere, on the other hand, initiate chemical alterations in the topmost centimetres of ice that, over geological timescales, may also affect deeper layers depending on the turnover processes at work. All surface interaction processes combine to produce the intriguing surface features of Ganymede, such as the separate dark and bright regions, the distribution of sulphur-bearing species, and the surface reservoir of molecular oxygen and ozone. The surface alteration processes discussed here are also the sources for Ganymede's atmosphere, the topic of the next chapter.

Acknowledgments

A. Galli, A. Vorburger, and P. Wurz wish to thank the Swiss National Science Foundation for their financial support.

References

Abdulgalil, A.G.M., Rosu-Finsen, A., Marchione, D., Thrower, J.D., Collings, M.P., McCoustra, M.R.S., 2017. Electron-Promoted Desorption from Water Ice Surfaces: Neutral Gas-Phase Products. ACS Earth and Space Chemistry 1, 209.

Andreas, E.L., 2007. New estimates for the sublimation rate for ice on the Moon. Icarus 186, 24–30.

Allioux, R., Louarn, P., André, N., 2013. Model of energetic populations at Ganymede, implications for an orbiter. Advances in Space Research 51, 1204–1212.

Aumayr, F., Winter, H., 2004. Potential sputtering. Phil. Trans. R. Soc. Lond. A, 362, 77–102.

Baragiola, R. A., 2003. Water ice on outer solar system surfaces: Basic properties and radiation effects. Planetary and Space Science 51, 953, doi.org/10.1016/j.pss.2003.05.007.

Bahr, D.A., Famfi, M., Vidal, R.A., Baragiola, R.A., 2001. Radiolysis of water ice in the outer solar system: Sputtering and trapping of radiation products. Journal of Geophysical Research 106, 33,285.

Bar-Nun, A., Herman, G., Laufer, D., Rappaport, M.L., 1985. Trapping and release of gases by water ice and implications for icy bodies. Icarus 63, 317, doi.org/10.1016/0019-1035(85)90048-X.

Batson, R.M., 1984. Voyager 1 and 2 Atlas of Six Saturnian Satellites (NASA-SP-474). Washington, DC: National Aeronautics and Space Administration (NASA).

Behr, P.R., Tribbett, P.D., Robinson, T.D., Loeffler, M.J., 2020. Compaction of porous H_2O ice via energetic electrons. The Astrophysical Journal 900, 147.

Boduch, P., Brunetto, R., Ding, J.J., Domaracka, A., Kaňuchová, Z., Palumbo, M.E., Rothard, H., Strazzulla, G., 2016. Ion processing of ices and the origin of SO_2 and O_3 on the icy surfaces of the icy jovian satellites. Icarus 277, 424.

Bohren, C.F., Albrecht, B.A., 1998. Atmospheric Thermodynamics. Oxford University Press, New York.

Boring, J.W., Garrett, J.W., Cummings, T.A., Johnson, R.E., Brown, W.L., 1984. Sputtering of solid SO_2. Nucl. Instrum. Methods B 1, 321–326.

Bottke, W.F., Vokrouhlický, D., Nesvorný, D., Moore, J.M., 2013. Black rain: The burial of the Galilean satellites in irregular satellite debris. Icarus 223, 775.

Brown, M.E., Hand, K.P., 2013. Salts and radiation products on the surface of Europa. The Astronomical Journal 145, 110.

Calvin, W. M., Johnson, R. E., and Spencer, J. R., 1996. O_2 on Ganymede: Spectral Characteristics and Plasma Formation Mechanisms. Geophysical Research Letters 23, 673–676.

Calvin, W. M., Johnson, R. E., and Spencer, J. R., 1996. O_2 on Ganymede: Spectral Characteristics and Plasma Formation Mechanisms. Geophysical Research Letters 23, 673–676.

Carlson, R.W., Johnson, R.E., Anderson, M.S., 1999. Sulfuric Acid on Europa and the Radiolytic Sulfur Cycle. Science 286, 97.

Carlson, R.W., Anderson, M.S., Johnson, R.E., Schulman, M.B., Yavrouian, A.H., 2002. Sulfuric Acid Production on Europa: The Radiolysis of Sulfur in Water Ice. Icarus 157, 456.

Carnielli, G., Galand, M., Leblanc, F., Modolo, R., Beth, A., Jia, X., 2020. Simulations of ion sputtering at Ganymede. Icarus 351, 113918.

Cassidy, T.A., Johnson R.E., 2005. Monte Carlo model of sputtering and other ejection processes within a regolith. Icarus 176, 499–507.

Cassidy, T., Coll, P., Raulin, F., Carlson, R.W., Johnson, R.E., Loeffler, M.J., Hand, K.P., Baragiola, R.A., 2010. Radiolysis and Photolysis of Icy Satellite Surfaces: Experiments and Theory. Space Science Reviews. doi:10.1007/s11214-009-9625-3.

Cassidy, T.A., Paranicas, C.P., Shirley, J.H., DaltonIII, J.B., Teolis, B.D., Johnson, R.E., Kamp, L., Hendrix, A.R., 2013. Magnetospheric ion sputtering and water ice grain size at Europa. Planetary and Space Science 77, 64–73.

Cooper, B.H., Tombrello, T.A., 1984. Enhanced erosion of frozen H_2O films by high energy ^{19}F ions. Radiation Effects 80, 203–221.

Cooper, J.F., Johnson, R.E., Mauk, B.H., Garrett, H.B., Gehrels, N., 2001. Energetic Ion and Electron Irradiation of the Icy Galilean Satellites. Icarus 149, 133–159.

Cooper, P.D., Moore, M.H., Hudson, R.L., 2005. Ozone Production in Irradiated Laboratory Ices Relevant to Europa and Ganymede. American Astronomical Society, DPS meeting #37, id.58.06, Bulletin of the American Astronomical Society, Vol. 37, p.752.

Davis, M.R., Meier, R.M., Cooper, J.F., Loeffler, M.J., 2021. The Contribution of Electrons to the Sputter-produced O_2 Exosphere on Europa. The Astrophysical Journal Letters 908, L53.

de Soria-Santacruz, M., Garrett, H. B., Evans, R. W., Jun, I., Kim, W., Paranicas, C., Drozdov, A. 2016. An empirical model of the high-energy electron environment at Jupiter. Journal of Geophysical Research: Space Physics, 121, 9732, doi.org/10.1002/2016JA023059.

Dones, L. et al., 2009. Icy satellites of Saturn: Impact cratering and age determination. In: Dougherty, M.K., Esposito, L.W., Krimigis, S.M. (Eds.), Saturn from CassiniHuygens. Springer-Verlag, Dordrecht, pp. 613–635.

Dukes, C. A., Chang, W.-Y., Famá, M., and Baragiola, R. A., 2011. Laboratory studies on the sputtering contribution to the sodium atmospheres of Mercury and the Moon. Icarus 212, 463–469.

Famá, M., Shi, J., Baragiola, R.A., 2008. Sputtering of ice by low-energy ions. Surface Science 602, 156.

Fatemi, S., Poppe, A.R., Khurana, K.K., Holmström, M., Delory, G.T., 2016. On the formation of Ganymede's surface brightness asymmetries: Kinetic simulations of Ganymede's magnetosphere. Geophysical Research Letters 43, 4745, doi:10.1002/2016GL068363.

Ferrari, C, Lucas, A., 2016. Low thermal inertias of icy planetary surfaces. Astronomy&Astrophysics 588, A133.

Frank, L. A., Paterson, W. R., Ackerson, K. L., Bolton, S. J., 1997. Low-energy electron measurements at Ganymede with the Galileo spacecraft: Probes of the magnetic topology. Geophysical Research Letters 24, 2159, doi.org/10.1029/97GL01632.

Fray, N., Schmitt, B., 2009. Sublimation of ices of astrophysical interest: A bibliographic review. Planetary and Space Science 57, 2053–2080.

Galli, A., Vorburger, A., Pommerol, A., Wurz, P., Jost, B., Poch, O., Brouet, Y., Tulej, M., Thomas, N., 2016. Surface charging of thick porous water ice layers relevant for ion sputtering experiments, Planetary and Space Science 126, 63–71.

Galli, A., Vorburger, A., Wurz, P., Tulej, M., 2017. Sputtering of water ice films: A re-assessment with singly and doubly charged oxygen and argon ions, molecular oxygen, and electrons. Icarus 291, 36, doi: 10.1016/j.icarus.2017.03.018.

Galli, A., Vorburger, A., Wurz, P., Cerubini, R., Tulej, M., 2018a. First experimental data of sulphur ions sputtering water ice. Icarus 312, 1, doi: 10.1016/j.icarus.2018.04.029.

Galli, A., Vorburger, A., Wurz, P., Pommerol, A., Cerubini, R., Jost, B., Poch, O., Tulej, M., and Thomas, N., 2018b. 0.2 to 10 keV electrons interacting with water ice: Radiolysis, sputtering, and sublimation. Planetary and Space Science 155, 91, doi: 10.1016/j.pss.2017.11.016.

Galli, A., Cerubini, R., Pommerol, A., Vorburger, A., Rubin, M., Wurz, P., Ligterink, N., Oza, A., Thomas, N., 2021. Electron-induced radiolysis of water ice and the buildup of O_2 in surfaces of icy moons and comets. *In preparation*

Grieves, G.A., Orlando, T.M., 2005. The importance of pores in the electron stimulated production of D_2 and O_2 in low temperature ice. Surface Science 593, 180.

Hand, K.P., and Carlson, R.W., 2011. H_2O_2 production by high-energy electrons on icy satellites as a function of surface temperature and electron flux. Icarus 215, 226, doi: 10.1016/j.icarus.2011.06.031.

Hansen, G. B., McCord, T. B., 2004. Amorphous and crystalline ice on the Galilean satellites: A balance between thermal and radiolytic processes. Journal of Geophysical Research 109, E01012, doi.org/10.1029/2003JE002149.

Haring, R.A., Pedrys, R., Oostra, D.J., Haring, A., De Vries, A.E., 1984. Reactive sputtering of simple condensed gases by keV ions III: kinetic energy distributions. Nuclear Instruments and Methods in Physics Research, B5, 483–488

Heide, H.G., 1984. Observations on ice layers. Ultramicroscopy 14, 271–278.

Howett, C.J.A., Spencer, J.R., Schenk, P., Johnson, R.E., Paranicas, C., Hurford, T.A., Verbiscer, A., Segura, M., 2011. A high-amplitude thermal inertia anomaly of probable magnetospheric origin on Saturn's moon Mimas. Icarus 216, 221.

Howett, C.J.A., Spencer, J.R., Hurford, T.A., Verbiscer, A., Segura, M., 2012. PacMan returns: An electron-generated thermal anomaly on Tethys. Icarus 221, 1084.

Johnson, R.E., 1990. Energetic Particle Interaction with Atmosheres and Surfaces (Springer, Berlin. 1990).

Johnson, R.E., 1997. Polar "Caps" on Ganymede and Io Revisited. Icarus 128, 469–471.

Johnson, R.E., Garrett, J.W., Boring, J.W., Barton, L.A., 1984. Erosion and Modification of SO_2 Ice by Ion Bombardment of the Surface of Io Application of Laboratory Data to the Sputtering of a Planetary Regolith. Journal of Geophysical Research 89, Supplement, B711.

Johnson, R.E., Burger, M.H., Cassidy, T.A., Leblanc, F., Marconi, M., Smyth, W.H., 2009. Composition and Detection of Europas Sputter-Induced Atmosphere. In: Pappalardo, R.T., McKinnon, W.B., Khurana, K.K. (Eds.), Europa. University of Arizona Press, Tucson.

Johnson, R.E., Carlson, R.W., Cooper, J.F., Paranicas, C., Moore, M.H., Wong, M.C., 2004. Radiation effects on the surfaces of the Galilean satellites. In: Bagenal, F. (Ed.), Jupiter: Atmosphere, Satellites and Magnetosphere. University of Arizona Press, Tucson.

Johnson, R.E., Jesser, W.A., 1997. Microatmospheres in the Surface of Ganymede. The Astrophysical Journal 480, L79.

Johnson, R.E. and Liu, M., 2010. Sputtering of Surfaces, Sputtering Data for H_2O ice, `http://people.virginia.edu/~rej/h2o.html`

Johnson, R.E., Oza, A.V., Leblanc, F., Schmidt, C., Nordheim, T.A., Cassidy, T.A., 2019. The Origin and Fate of O_2 in Europa's Ice: An Atmospheric Perspective. Space Science Reviews 215, 20.

Jones, B.M., Kaiser, R.I., Strazzulla, G., 2014. UV-VIS, infrared, and mass spectroscopy of electron irradiated frozen oxygen and carbon dioxide mixtures with water. The Astrophysical Journal 781, 85.

Jun, I., Garrett, H. B., Cassidy, T. A., Kim, W., Dougherty, L., 2019. Updating the Jovian electron plasma environment. IEEE Transactions on Plasma Science 47, 3915, doi.org/10.1109/TPS.2019.2901681.

Khurana, K.K., Pappalardo, R.T., Murphy, N., Denk, T., 2007. The origin of Ganymede's polar caps. Icarus 191, 193.

Kivelson, M.G., Bagenal, F., Kurth, W.S., Neubauer, F.M., Paranicas, C., Saur, J., 2004. Magnetospheric interactions with satellites. In: Bagenal, F., Dowling, T., McKinnon, W.K. (Eds.), Jupiter, The Planet, Satellites and Magnetosphere. Cambridge University Press, Cambridge, Chapter 21.

Krüger, H., Krivov, A.V., Grün, E., 2000. A dust cloud of Ganymede maintained by hypervelocity impacts of interplanetary micrometeoroids. Planetary and Space Science 48, 1457.

Küstner, M., Eckstein, W., Dose, V., Roth, J, 1998. The influence of surface roughness on the angular dependence of the sputter yield. Nucl. Instrum. Methods B 145, 320–331.

Laufer, D., Bar-Nun, A., Greenberg, A.N., 2017. Trapping mechanism of O_2 in water ice as first measured by Rosetta spacecraft. Monthly Notices of the Royal Astronomical Society 469, S818, doi: 10.1093/mnras/stx3359.

Leblanc, F. Oza, A.V., Leclercq, L., Schmidt, C., Cassidy, T., Modolo, R., Chaufray, J.Y, Johnson, R.E., 2017. On the orbital variability of Ganymedes atmosphere. Icarus 293, 185.

Ligier, N., Paranicas C., Carter, J., Poulet, F., Calvin, W.M., Nordheim, T.A., Snodgrass, C., Ferellec, L., 2019. Surface composition and properties

of Ganymede: Updates from ground-based observations with the near-infrared imaging spectrometer SINFONI/VLT/ESO. Icarus 333, 496.

Liuzzo, L., Poppe, A.R., Paranicas, C., Fatemi, S., Simon, S., 2020. Variability in the Energetic Electron Bombardment of Ganymede. Journal of Geophysical Research: Space Physics, 125, e2020JA028347.

Loeffler, M.J., Teolis, B.D., Baragiola, R.A., 2006. A Model Study of the Thermal Evolution of Astrophysical Ices. The Astrophysical Journal 639, L103.

Loeffler, M.J., Hudson, R.L., Moore, M.H., Carlson, R.W., 2011. Radiolysis of sulfuric acid, sulfuric acid monohydrate, and sulfuric acid tetrahydrate and its relevance to Europa. Icarus 215, 370.

Loeffler, M.J., Hudson, R.L., 2012. Thermal regeneration of sulfuric acid hydrates after irradiation. Icarus 219, 561.

Loeffler, M. J., Tribbett, P. D., Cooper, J. F., Sturner, S. J. 2020. A possible explanation for the presence of crystalline H_2O-ice on Kuiper Belt objects. Icarus 351, 113,943. doi.org/10.1016/j.icarus.2020.113943.

Marconi, M.L., 2007. A kinetic model of Ganymede's atmosphere. Icarus 190, 155.

Mauk, B. H., Mitchell, D. G., McEntire, R. W., Paranicas, C. P., Roelof, E. C., Williams, D. J., Krimigis, S. M., Lagg, A., 2004. Energetic ion characteristics and neutral gas interactions in Jupiter's magnetosphere. Journal of Geophysical research 109, A09S12, doi:10.1029/2003JA010270.

McCord, T.B., Orlando, T.M., Teeter, G., Hansen, G.B., Sieger M.T., Petrik, N.G., van Keulen, L., 2001. Thermal and radiation stability of the hydrated salt minerals epsomite, mirabilite, and natron under Europa environmental conditions. Journal of Geophysical Research, 106, 3311.

McEwen, A.S., 1986. Exogenic and endogenic albedo and color patterns on Europa. Journal of Geophysical Research, 91, 8077.

Meier, R. M., and Loeffler, M. J., 2020. Sputtering of water ice by keV electrons at 60 K. Surface Science 691, 121509, doi: 10.1016/j.susc.2019.121509.

Miljković, K., Hillier, J.K., Mason, N.J., Zarnecki, J.C., 2012. Models of dust around Europa and Ganymede. Planetary and Space Science 70, 20.

Moore, M.H., Hudson, R.L., Carlson, R.W., 2007. The radiolysis of SO_2 and H_2S in water ice: Implications for the icy jovian satellites. Icarus 189, 409.

Muntean, E. A., Lacerda, P., Field, T. A., Fitzsimmons, A., Fraser, W. C., Hunniford, A. C., McCullough, R. W., 2016. A laboratory study of water ice erosion by low-energy ions. Mon. Not. R. Astron. Soc. 462, 3361.

Mura, A., Adriani, A., Sordini, R., Sindoni, G., Plainaki, C., Tosi, F., et al. 2020. Infrared observations of Ganymede from Juno/Jovian infrared auroral mapper. Journal of Geophysical Research: Planets, 125, e2020JE006508.

Murphy, D.M., Koop, T., 2005. Review of the vapour pressures of ice and supercooled water for atmospheric applications. Quart. J. R. Meteor. Soc. 131, 1539.

Mutzke A., Schneider R., Bizyukov, I. 2009. SDTrimSP-2D studies of the influence of mutual flux arrangement on erosion and deposition. Journal of Nuclear Materials 390-391, 115.

Noll, K.S., Johnson, R.E., Lane, A.L., Domingue, D.L., Weaver, H.A., 1996. Detection of Ozone on Ganymede. Science, 273, 341.

Nordheim, T.A., Hand, K.P., Paranicas, C., Howett, C.J.A., Hendrix, A.R., Jones, G.H., Coates, A.J., 2017. The near-surface electron radiation environment of Saturn's moon Mimas. Icarus 286, 56.

Orlando, T.M., Sieger, M.T., 2003. The role of electron-stimulated production of O_2 from water ice in the radiation processing of outer solar system surfaces. Surface Sciences 528, 1.

Orton, G.S., Spencer, J.R., Travis, L.D., Martin, T.Z., Tamppari, L.K., 1996. Galileo Photopolarimeter-Radiometer Observations of Jupiter and the Galilean Satellites. Science 274, 389.

Pappalardo, R.T. et al., 2004. Geology of Ganymede. In: Bagenal, F., Dowling, T., McKinnon, W.K. (Eds.), Jupiter, The Planet, Satellites and Magnetosphere. Cambridge University Press, Cambridge, pp. 363–396.

Paranicas, C., Mauk, B.H., Ratliff, J.M., Cohen, C., Johnson, R.E., 2001. The ion environment near Europa and its role in surface energetics. Geophysical Research Letters 29, 10.1029/2001GL014127.

Petrik, N. G., Kavetsky, A. G., Kimmel, G.A., 2006. Electron-Stimulated Production of Molecular Oxygen in Amorphous Solid Water. J. Phys. Chem. B2006,110,2723-2731

Plainaki, C., Milillo, A., Mura, A., Orsini, S., Massetti, S., Cassidy, T., 2012. The role of sputtering and radiolysis in the generation of Europa exosphere. Icarus 218, 956.

Plainaki, C., Milillo, A., Massetti, S., Mura, A., Jia, X., Orsini, S., Mangano, V., De Angelis, E., Rispoli, R., 2015. The H_2O and O_2 exospheres of Ganymede: The result of a complex interaction between the jovian magnetospheric ions and the icy moon. Icarus 245, 306.

Plainaki, C., Massetti, S., Jia, X., Mura, A., Milillo, A., Grassi, D., Sindoni, G., D'Aversa, E., and Filacchione, G., 2020a. Kinetic Simulations of the Jovian Energetic Ion Circulation around Ganymede. The Astrophysical Journal 900, 74.

Plainaki, C., et al., 2020b. Preliminary estimation of the detection possibilities of Ganymedes watervapor environment with MAJIS. Planetary and Space Science 191, 105004.

Poppe, A.R., 2016. An improved model for interplanetary dust fluxes in the outer Solar System. Icarus 264, 369.

Poppe, A.R., Fatemi, S., Khurana, K. K., 2018. Thermal and Energetic Ion Dynamics in Ganymedes Magnetosphere. Journal of Geophysical Research: Space Physics 123, 4614.

Roth, L., Ivchenko, N., Gladstone, G.R., Saur, J., Grodent, D., Bonfond, B., Molyneux, P.M., Retherford, K.D., 2021. A sublimated water atmosphere on Ganymede detected from Hubble Space Telescope observations. Nature Astronomy, doi:10.1038/s41550-021-01426-9.

Schaible, M. J., Johnson, R. E., Zhigilei, L. V., Piqueux, S., 2017. High energy electron sintering of icy regoliths: Formation of the Pac-Man thermal anomalies on the icy Saturnian moons. Icarus 285, 211, doi.org/10.1016/j.icarus.2016.08.033.

Shematovich, V.I.Neutral Atmosphere Near the Icy Surface of Jupiters Moon Ganymede. Solar System Research 50, 262.

Shi, M., Baragiola, R.A., Grosjean, D.E., Johnson, R.E., Jurac, S., Schou, J., 1995. Sputtering of water ice surfaces and the production of extended neutral atmospheres. Journal of Geophysical Research 100, 26387.

Shi, J., Raut, U., Kim, J.-H., Loeffler, M., Baragiola, R.A., 2011. Ultraviolet photon-induced synthesis and trapping of H_2O_2 and O_3 in porous water ice films in the presence of ambient O_2: Implications for extraterrestrial ice. The Astrophysical Journal Letters 783.

Shirley, J.H., Dalton III, J.B., Prockter, L.M., Kamp, L.W., 2010. Europa's ridged plains and smooth low albedo plains: Distinctive compositions and compositional gradients at the leading sidetrailing side boundary. Icarus, 210, 358–384.

Sivaraman, B., Jamieson, C.S., Mason, N.J., Kaiser, R.I., 2007. Temperature-dependent Formation of Ozone in Solid Oxygen by 5 keV Electron Irradiation and Implications for Solar System Ices. The Astrophysical Journal 669, 1414.

Spencer, J.R., 1987. Thermal segregation of water ice on the Galilean satellites. Icarus 69, 297.

Spencer, J.R., Calvin, W.M., Person, M.J., 1995. Charge-coupled device spectra of the Galilean satellites: Molecular oxygen on Ganymede. Journal of Geophysical Research 100, 19049.

Spencer, J.R., Calvin, W.M., and Person, M.J., 2002. Condensed O_2 on Europa and Callisto. The Astronomical Journal 124, 3400, doi: 10.1086/344307.

Stephan, K., Hibbitts, C.A., Jaumann, R., 2020. H_2O-ice particle size variations across Ganymede's and Callisto's surface. Icarus 337, 113440.

Strazzulla, G., Baratta, G.A., Leto, G., Gomis, O., 2007. Hydrate sulfuric acid after sulfur implantation in water ice. Icarus 192, 623.

Teolis, B.D., Loeffler, M.J., Raut, U., Famá, M., Baragiola, R.A., 2006. Ozone synthesis on the icy satellites. The Astrophysical Journal 644, L141.

Teolis, B.D., Shi, J., Baragiola, R.A., 2009. Formation, trapping, and ejection of radiolytic O_2 from ion-irradiated water ice studied by sputter depth profiling. The Journal of Chemical Physics 130, 134704.

Teolis, B.D., Jones, G.H., Miles, P.F., Tokar, R.L., Magee, B.A., Waite, J.H., Roussos, E., Young, D.T., Crary, F.J., Coates, A.J., Johnson, R.E., Tseng, W.-L., Baragiola, R.A., 2010. Cassini finds an oxygen–carbon dioxide atmosphere at Saturns icy moon Rhea (Supporting Online Material), Science, 330, 1813.

Teolis, B.D., Plainaki, C., Cassidy, T.A., Raut, U., 2017. Water Ice Radiolytic O_2, H_2, and H_2O_2 Yields for Any Projectile Species, Energy, or Temperature: A Model for Icy Astrophysical Bodies. Journal of Geophysical Research: Planets 122, 2017JE005285.

Trumbo, S. K., Brown, M. E., Hand, K.P., 2019. Sodium chloride on the surface of Europa. Science Advances, 5, eaaw7123

Turc, L. Leclercq, L., Leblanc, F., Modolo, R., Chaufray, J.-Y., 2014. Modelling Ganymedes neutral environment: A 3D test-particle simulation, Icarus 229, 157.

Vidal R.A., Bahr, D., Baragiola, R.A., Peters, M., 1997. Oxygen on Ganymede: Laboratory Studies. Science 276, 1839.

Vorburger, A., Wurz, P., Lammer, H., Barabash, S., Mousis, O., 2015. Monte-Carlo Simulation of Callisto's Exosphere. Icarus, 262, 14–29.

Vorburger, A., Wurz, P., 2018. Europa's ice-related atmosphere: The sputter contribution. Icarus 311, 135–145.

Westley, M.S., Baragiola, R.A., Johnson, R.E., Baratta, G.A., 1995. Photodesorption from low-temperature water ice in interstellar and circumsolar grains. Nature 373, 405.

Wiens, R.C., Burnett, D.S., Calaway, W.F., Hansen, C.S., Lykke, K.R., Pellin, M.J., 1997. Sputtering Products of Sodium Sulfate: Implications for Io's Surface and for Sodium-Bearing Molecules in the Io Torus. Icarus 128, 386.

Zheng, W.-J., Jewitt, D., Kaiser, R.I., 2006. Formation of hydrogen, oxygen, and hydrogen peroxide in electron-irradiated crystalline water ice. The Astrophysical Journal 639, 534.

Ziegler, J.F., Biersack, J.P., Ziegler, M.D., 2008. "SRIM – The Stopping and Range of Ions in Matter". Vol. 5 (SRIM Co., Chester, MD, 2008).

Zolotov, M.Y., Shock, E.L., 2001. Composition and stability of salts on the surface of Europa and their oceanic origin. Journal of Geophysical Research 106, 32815.